scientific reports

Check for updates

OPEN

Transcriptome combined with Mendelian randomization to identify key genes related to polyamine metabolism in childhood obesity and elucidate their molecular regulatory mechanisms

Manman Sun, Pei Zhang, Sheng Yang, Yunyang Qiao, Xuepo Shen, Jialing Ji✉ & Ling Ding✉

Currently, research has found a close correlation between childhood obesity (CO) and elevated levels of polyamines in the bloodstream. Thus, the identification of key genes associated with polyamines metabolism in CO could offer fresh insights for clinical management of CO. This study utilized two datasets from public databases (GSE205668 and GSE104815) and 59 polyamines metabolism-related genes (PMRGs) to screen for candidate genes. Subsequently, candidate key genes were selected using Mendelian randomization (MR) analysis, and machine learning algorithms were employed to obtain intersecting feature genes based on the MR results. Then key genes were identified through expression validation. Finally, we conducted research on the key genes including gene set enrichment analysis (GSEA), immune infiltration, and transcription factor(TF)-mRNA network. Differential analysis identified 432 candidate genes linked to childhood obesity and polyamine metabolism, with 4 key genes showing causal relationships. Specifically, *WWC1*, *NPL*, and *LAPTM5* as risk factors [odd ratio (OR) > 1], while GPAT3 (OR < 1) was identified as a protective factor for CO. Machine learning algorithms pinpointed 3 feature genes (*WWC1*, *NPL*, and *GPAT3*) with significant differential expression and consistent trends. GSEA revealed ribosome and lysosome pathways linked to key genes. MITF regulated these genes in the TF-mRNA network. Twelve immune cell types, mostly correlating with key genes, were identified. We identified 3 key genes (*WWC1*, *NPL*, and *GPAT3*) related to polyamine metabolism in CO. Additionally, we investigated their potential biological functions and regulatory mechanisms, aiming to provide new theoretical basis for the treatment and diagnosis of CO.

Keywords Childhood obesity, Polyamines metabolism, Mendelian randomization, Transcriptome

As one of the global public health problems, especially childhood obesity (CO), its incidence rate has increased year by year, which has become a new challenge in the field of global public health[1]. In addition, with the continuous development of China's social economy, the unhealthy dietary habits of high sugar, high fat, and high salt as well as a lifestyle that relies on developed transportation and the internet and lacks exercise, have led to an increasing incidence of CO year by year, and the situation is not optimistic[2]. A study has discovered that obese children and adolescents were approximately five times more likely to be obese in adulthood compared with those who were not obese[3]. 0bese children are negatively affected to varying degrees both physically and psychologically. Previous studies have shown that children who are obese have a significantly increased risk of developing mental health problems and of dying as an adult[4]. On the other hand, obesity not only affects the growth and development of children, but also increases the incidence and mortality of cardiovascular disease,

Department of Pediatrics, the Fourth Affiliated Hospital of Nanjing Medical University, Nanjing, China. ✉email: melodyjialing@163.com; 414846722@qq.com

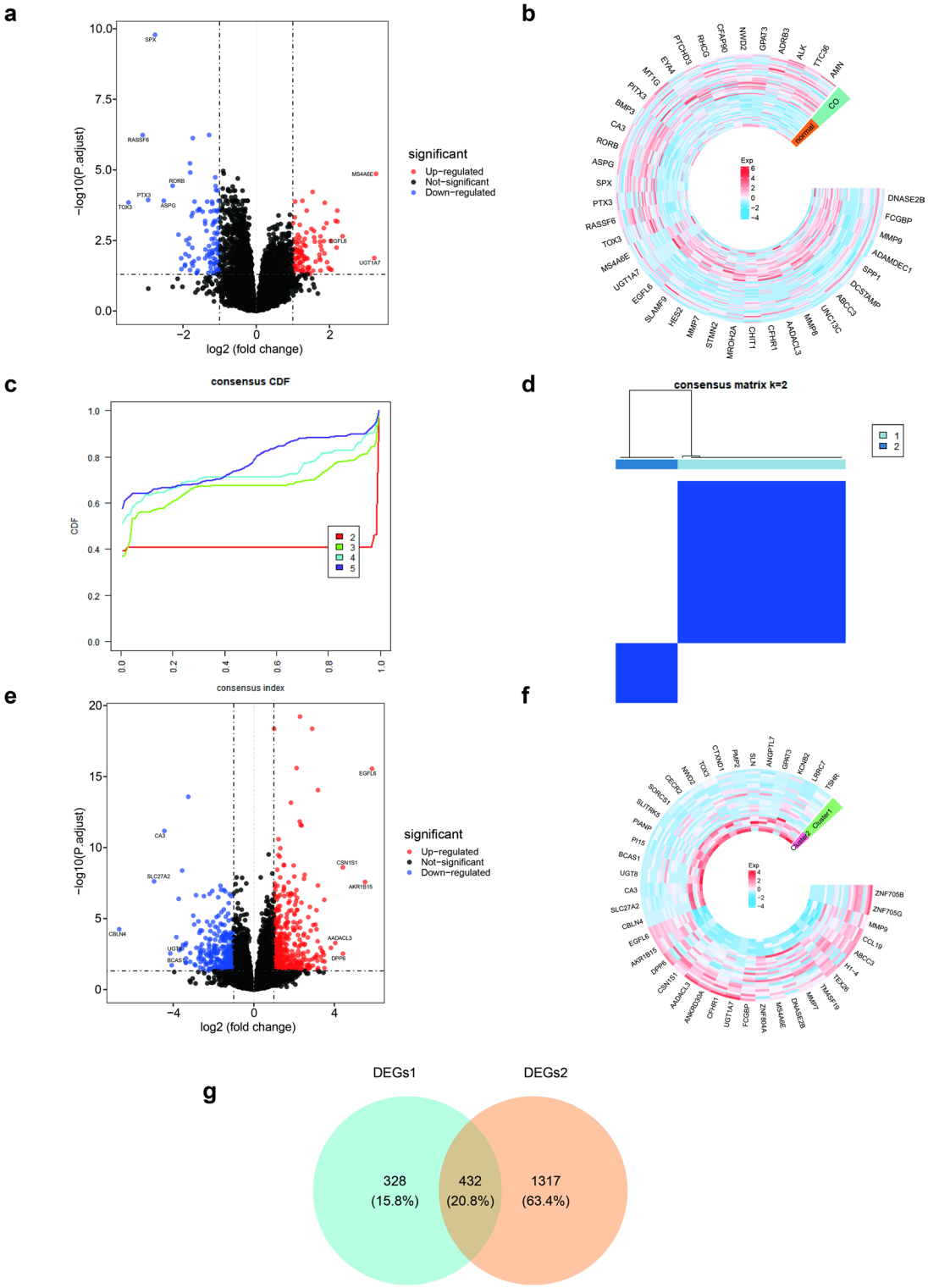

non-alcoholic fatty liver disease, type 2 diabetes, and some cancers (e.g. breast cancer) in adult life[5]. Although changing unhealthy dietary habits and increasing physical activity are effective methods for treating obesity, they are difficult to adhere to, especially for children and patients with severe obesity or multiple complications[6]. In terms of drug intervention, current research focuses on drugs that simulate physiological logic, such as drugs that regulate appetite, metabolism, and insulin sensitivity, to help children control their weight. These drugs may produce effects by affecting brain signaling, adipocyte metabolism, or insulin signaling pathways[7]. However, it is worrying that most obesity treatment drugs have serious gastrointestinal side effects, such as abdominal pain, increased bowel movements, pancreatitis, and even psychological side effects such as insomnia and anxiety[8]. Their safety and long-term effects still need more research to verify. Therefore, it is necessary to explore the potential development mechanism of CO in order to develop effective treatment strategies.

◀**Fig. 1**. Identifying candidate genes. (**a, b**) Volcano plot of DEGs1 in the training set (red dots indicate up-regulated gene expression, blue dots indicate down-regulated gene expression, black dots indicate no significant difference in genes, and the top 10 differentially expressed genes of |log2FC| are marked simultaneously) and annular heat map of the top 20 differentially expressed genes for up-regulation and down-regulation respectively (the higher the expression level, the redder the color; the lower the expression level, the bluer the color). (**c, d**) Cumulative Distribution Function of consensus clustering in GSE205668 Dataset (The ordinate (y-axis) represents the cumulative distribution function, which shows the cumulative proportion of sample pairs with consensus index values less than or equal to a given threshold. A consensus index of 1 means that a pair of samples was always clustered together. A consensus index of 0 means they were never clustered together, indicating they belong to different clusters). Different colors represent different numbers of classes. Red is divided into two classes, green is divided into three classes, and so on) and consensus clustering heat map (the color indicates the consensus index. The darker the white color, the more difficult it is to cluster; the darker the blue color, the easier it is to cluster into one class). (**e, f**) Using two subtypes as groups, volcano plot and heat map of DEGs2 in the GSE205668 dataset. (**g**) Venn diagram of candidate genes (intersection of DEGs1 and DEGs2).

Polyamines are organic compounds with two or more amino groups which has a positive charge at physiological pH. It is able to interact with negatively charged macromolecules DNA, RNA, and proteins etc. in the cell through the generation of static electricity, mainly including putrescine, spermine, and spermidine[9]. Polyamine metabolism refers to the process of synthesis, release, and degradation of polyamines in the body, which plays an important role in the occurrence, development, and diagnosis of various diseases[10]. Studies have shown that the metabolites of polyamines are significantly associated with the progression of cardiovascular diseases such as vascular function and arteriosclerosis[11]. Previous studies also have found that obese children have elevated levels of polyamines, which are associated with markers of oxidation-phosphorylation and angiogenesis[12]. Furthermore, polyamines can regulate gene expression, affect DNA and protein synthesis, and thus regulate cell growth and differentiation[13]. Polyamines also play an important role in regulating lipid metabolism. Abnormal polyamine metabolism is closely related to insulin resistance and obesity[13]. However, research on the relationship between polyamine metabolism and the progression of CO is still lacking. Therefore, exploring the mechanism of action of polyamines metabolism-related genes (PMRGs) in CO can help understand the pathogenesis and molecular mechanisms of the disease, and provide targets for clinical diagnosis and treatment.Mendelian randomization (MR) is a statistical method that uses genetic variation to study the causal relationship between exposure factors (such as certain biomarkers, lifestyles, etc.) and disease or health outcomes[1]. MR is considered the 'most natural' randomized controlled trial, attributed to the allele distribution from parent to offspring Genes which are randomly assigned and freely combined, and genotypes remain stable after birth[14]. Compared to the previous randomized controlled analysis, it breaks through the limitations of traditional randomized controlled studies and avoids the interference of confounding factors. With the development of basic Mendelian theory and the increase of practical applications, MR analysis can be used to evaluate the correlation and causal relationship between PMRGs and CO.

This study combines transcriptomics and MR data, using a series of bioinformatics methods to identify key genes related to polyamine metabolism in CO. Gene set enrichment analysis (GSEA), immune infiltration, and transcription factor (TF)-mRNA network were also studied, and the potential molecular mechanisms of key genes were elucidated, which may provide new ideas for the clinical diagnosis, prevention, and treatment of CO.

Results

Identifying candidate genes

In this study, we used Consensus Clustering to group the data. The coherence of this analytical approach allowed some genes to be identified at different stages of the analysis, thus presenting them as overlapping phenomena in Fig. 1. First, in the training cohort, we identified 760 DEGs1 related to CO through expression difference analysis (408 up-regulated; 352 down-regulated) (Fig. 1a-b). Subsequently, consistency clustering analysis was performed using the expression data of 59 polyamine metabolism-related genes (PMRGs) from 26 CO samples in the GSE205668 dataset. The 26 CO samples were divided into two subtypes: Cluster 1, which included 7 samples, and Cluster 2, which included 19 samples. (Fig. 1c-d). Next, differential expression analysis was performed on the two subtypes, resulting in the identification of 1,749 DEGs2 (982 up-regulated genes, 767 down-regulated genes) (Fig. 1e-f). Finally, the intersection of the two sets of DEGs yielded 432 genes related to polyamine metabolism in CO, which were chosen as candidate genes for further analysis (Fig. 1g).

Functional enrichment and protein interaction analysis of candidate genes

To comprehensively understand the potential biological roles and molecular mechanisms underlying the candidate genes, the functional enrichment and protein interaction analysis of candidate genes were conducted. A GO enrichment analysis of the candidate genes yielded 1,350 significant results ($p < 0.05$) (Fig. 2a). In terms of biological processes (BP), 1,131 results were obtained, such as regulation of leukocyte mediated immunity, regulation of immune effector process, etc.; in molecular functions (MF), there were 127 results, such as immune receptor activity, fibronectin binding etc.; and in cellular components (CC), there were 92 results, such as external side of plasma membrane, MHC class II protein complex, etc. Additionally, in the KEGG pathway analysis, 58 relevant pathways ($p < 0.05$) were identified, showing significant associations of the candidate genes with metabolic pathways such as rheumatoid arthritis, cell adhesion molecules, etc. (Fig. 2b). Subsequently, a PPI network was constructed to explore the interactions among 432 candidate genes. After removing 96 isolated

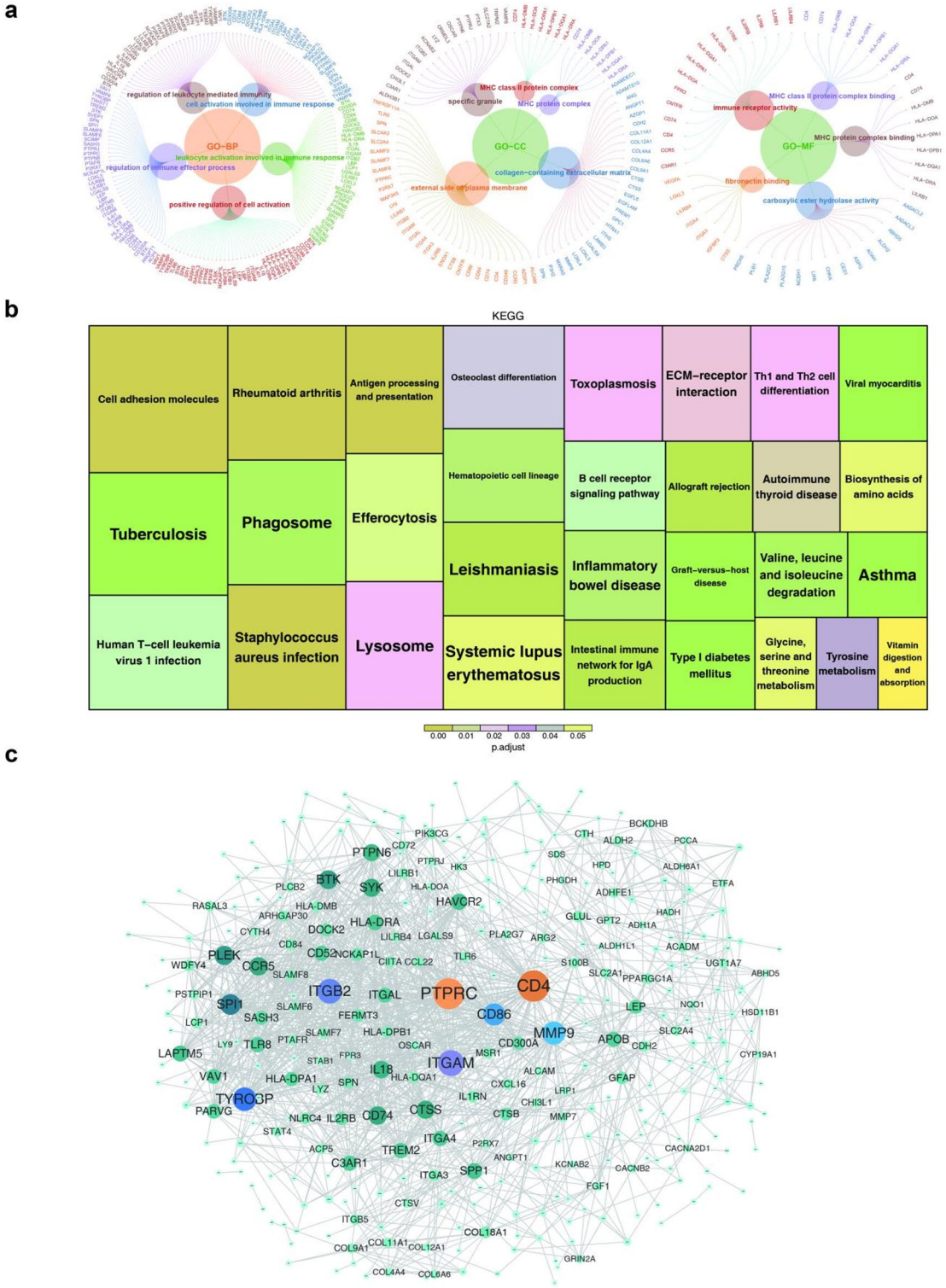

Fig. 2. Functional enrichment analysis and PPI network construction. (**a**) GO enrichment analysis of candidate genes. (**b**) KEGG enrichment analysis of candidate genes, showing the top 30 pathways. (**c**) Protein-protein interaction relationship network (lines represent the interaction relationship between them.

nodes, a PPI network with 336 nodes and 1,487 edges was successfully constructed, indicating a certain level of interaction among these 336 genes (Fig. 2c). Notably, PTPRC and CD4 had important regulatory roles in the PPI network constituted by candidate genes.

MR analysis to identified the candidate key genes

In order to explored the causal relationship between polyamine metabolism-related genes and CO, a two-sample Mendelian randomization (MR) analysis was carried out with 432 candidate genes as the exposure factors and CO as the outcome event. We conducted a filtering analysis using eQTL and GWAS dataset obtained from public databases, resulting in 327 eQTL data (exposure factor data) meeting the analysis criteria, including 1,599 SNPs. Then, the strength of each IV was assessed using the F statistic, yielding 1,106 IVs for MR analysis. MR analysis revealed a causal mechanism between the eQTL of 8 genes and the CO (IVW $p < 0.05$) (Fig. 3a; Table 1). Screening of the expression levels of these 8 genes in the disease (OR > 1 and log2FC > 0 or OR < 1 and log2FC < 0) identified 4 significant genes (*WWC1*, *NPL*, *GPAT3*, *LAPTM5*) as candidate key genes. Specifically, *WWC1* (OR = 1.183, 95% Confidence Interval (CI):1.015–1.337, $p = 0.031$), *NPL* (OR = 1.298, 95% CI:1.068–1.579, $p = 0.009$), and *LAPTM5* (OR = 1.130, 95% CI:1.019–1.253, $p = 0.020$) as risk factors, while *GPAT3* (OR = 0.663266489, 95% CI:0.457–0.964, $p = 0.03116954$) was identified as a protective factor for CO.

Additionally, the scatter plot also showed same results of MR study, *GPAT3* had a negative slope of the fitted, while *WWC1*, *NPL*, and *LAPTM5* had a positive slope of the fitted (Fig. 3b). Next, forest map results showed that MR effect sizes of *WWC1*, *NPL*, and *LAPTM5* was greater than 0, while the effect size of *GPAT3* was less than 0 in the IVW method (Fig. 3c). The funnel plot results were presented in Fig. 3d, IV was roughly equally distributed along both sides of the IVW line, this result means the MR study conformed to Mendel's second law.

Additionally, a series of sensitivity analyses were conducted to evaluate the reliability of the analysis results. Firstly, heterogeneity testing indicated no heterogeneity between the 4 exposure factors and the outcome, demonstrating the reliability of our MR results. (Table 2). Subsequently, the use of two functions (MR-Egger and MR-PRESSO) to test for horizontal pleiotropy yielded consistent results, confirming the absence of horizontal pleiotropy between these 4 candidate key genes and the outcome variables (Tables 3 and 4). Finally, through LOO analysis, no significantly biased points were identified, indicating the reliability of the results (Fig. 3E). Ultimately, a directional test was conducted on the MR results, revealing a "TRUE" directional relationship ($p < 0.05$) (Table 5). The four genes that had a significant causal relationship with CO obtained from Mendelian randomization analysis were regarded as candidate key genes.

Selection of key genes and validation of their diagnostic value

To further explored the characteristics and importance of the four candidate key genes obtained through Mendelian randomization analysis, we performed LASSO and Boruta analyses on them. Through LASSO regression, we identified 3 feature genes—*WWC1*, *NPL*, and *GPAT3*—when the lambda.min was 0.0481 (achieving the lowest error rate) as the feature genes (Fig. 4a). Subsequently, Boruta analysis on 4 candidate key genes in the training cohort yielded 3 feature genes: *GPAT3*, *WWC1*, and *NPL* (Fig. 4b).

Next, taking the intersection of the feature genes obtained from LASSO and Boruta, we obtained 3 intersecting genes: *WWC1*, *NPL*, and *GPAT3* (Fig. 4c). We observed that the expression trends of these three intersecting genes were consistent and significantly different in both the training and validation cohorts. *WWC1* and *NPL* showed elevated expression levels in the CO group, whereas *GPAT3* exhibited higher expression in the control group. Thus indicating their significance as key genes related to polyamine metabolism in CO (Fig. 4d). Finally, through ROC analysis, we found that the AUC values of the 3 key genes (*WWC1*, *NPL*, *GPAT3*) in the two datasets were all greater than 0.7, indicating that these 3 key genes had good accuracy in distinguishing between CO and healthy samples (Fig. 4e).

GSEA and construction of GGI and molecular regulatory network

To further understand the biological functions of the three key genes in CO, Gene Set Enrichment Analysis (GSEA) was performed to search for the regulatory pathways or biological functions related to the expression of these three genes. In the GSEA, we identified 108 pathways associated with *WWC1*, 183 pathways associated with *NPL*, and 125 pathways associated with *GPAT3*. There were top 5 pathways in *WWC1*, *NPL*, and *GPAT3* were displayed (Fig. 5a). Notably, 3 key genes common enriched in ribosome and lysosome pathways. Utilizing the GeneMANIA database (http://www.genemania.org), we constructed a GGI network and presented the top 20 genes with the strongest functional similarity (Fig. 5b). These genes were involved in biological processes such as glycerophospholipid biosynthetic process, phospholipid biosynthetic process, O-acyltransferase activity, lysophospholipid acyltransferase activity, and carboxylic acid catabolic process.

Subsequently, we utilized NetworkAnalyst to identify 72 TFs corresponding to 3 key genes and constructed an mRNA-TF network consisting of 75 nodes and 92 edges, with MITF concurrently regulating three key genes (Fig. 5c).

Following this, we predicted 186 target miRNAs interacting with the key genes using the miRWalk database. Subsequently, we obtained 17 key lncRNAs (upstream lncRNAs targeting the miRNAs) from public databases and visualized the competing endogenous RNA (ceRNA) regulatory network using Cytoscape. This network included 3 key genes, 7 miRNAs, and 17 lncRNAs, with a total of 94 edges (Fig. 5d). Among them, *MALAT1* simultaneously regulated *GPAT3* and *WWC1*, while *NEAT1* simultaneously regulated *NPL* and *GPAT3*.

Immunological infiltration analysis of key genes

To investigate the differences in immune cell infiltration between CO and healthy control samples, we calculated the infiltration of 28 types of immune cells in all samples from dataset GSE205668 (Fig. 6a). Through Wilcoxon rank sum tests, we found significant differences ($P < 0.05$) in the infiltration of 12 types of immune cells between

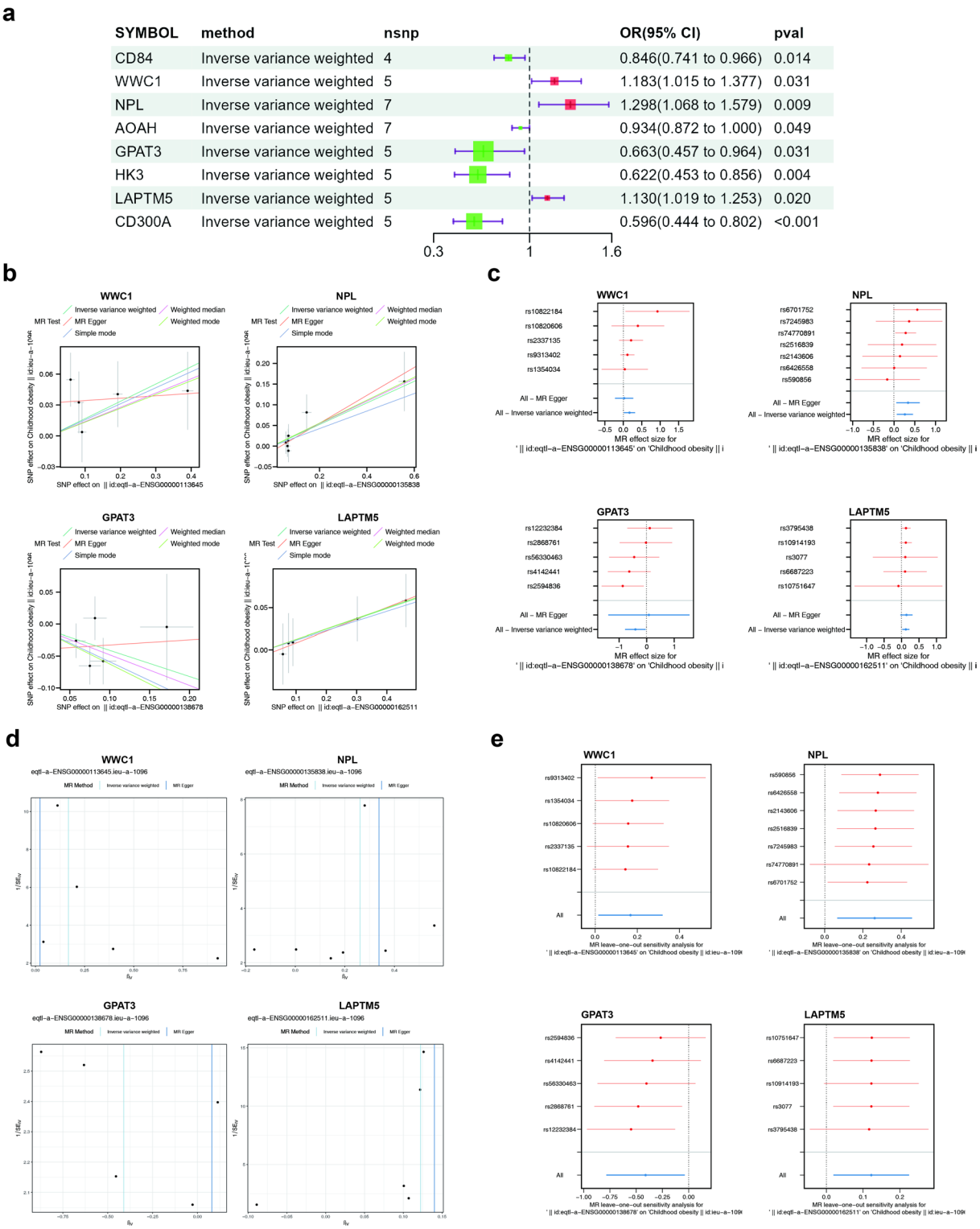

Fig. 3. MR analysis. (**a**) IVW forest plot shows that the univariate MR shows the causal mechanism between the eqtl exposure factors of 8 genes and CO ($P<0.05$ for IVW). (**b**) Scatter plot of MR (the slope of the fitted line is positive, indicating a risk factor; the slope of the fitted line is negative, indicating a protective factor; the size of the intercept indicates the influence of confounding factors). (**c**) Forest plot of MR, the SNP points on the left side of the dashed line indicate a decrease (safety factor), while SNP points on the right side of the dashed line indicate an increase (risk factor). (**d**) Funnel plot of MR. If the samples are symmetrically distributed on both sides of the IVW line, MR conforms to the random grouping of Mendel's second law. (**e**) Display of MR Leave-one-out analysis.

SYMBOL	Methods	nsnp	b	or	pval	log2FC
CD84	Inverse variance weighted	4	-0.166700879	0.846452765	0.013707026	1.053651238
WWC1	Inverse variance weighted	5	0.167757633	1.18264994	0.03107279	0.962410168
NPL	Inverse variance weighted	7	0.261100543	1.298358199	0.008841518	0.813572247
AOAH	Inverse variance weighted	7	-0.068484219	0.933808197	0.049290705	0.891478407
GPAT3	Inverse variance weighted	5	-0.410578426	0.663266489	0.03116954	-1.822564924
HK3	Inverse variance weighted	5	-0.474054406	0.622473385	0.003521294	0.800721959
LAPTM5	Inverse variance weighted	5	0.122185343	1.129963513	0.020152426	0.607085707
CD300A	Inverse variance weighted	5	-0.516822214	0.596412812	0.000625203	0.657782081

Table 1. MR-IVW results between eQTL for 8 genes and CO.

SYMBOL	id.exposure	method	Q	Q_df	Q_pval
WWC1	eqtl-a-ENSG00000113645	Inverse variance weighted	3.879386112	4	0.42257519
NPL	eqtl-a-ENSG00000135838	Inverse variance weighted	2.730554793	6	0.841825128
GPAT3	eqtl-a-ENSG00000138678	Inverse variance weighted	3.909660201	4	0.418370052
LAPTM5	eqtl-a-ENSG00000162511	Inverse variance weighted	0.117376676	4	0.99834376

Table 2. MR heterogeneity test results between eQTL for 4 genes and CO.

SYMBOL	id.exposure	egger_intercept	se	pval
WWC1	eqtl-a-ENSG00000113645	0.031987872	0.022027226	0.24237692
NPL	eqtl-a-ENSG00000135838	-0.012334499	0.016742621	0.494390249
GPAT3	eqtl-a-ENSG00000138678	-0.040692444	0.060141247	0.547148351
LAPTM5	eqtl-a-ENSG00000162511	-0.005843926	0.023277888	0.817988312

Table 3. MR-Egger horizontal Pleiotropy test between eQTL for 4 genes and CO.

SYMBOL	id.exposure	RSSobs	Pvalue
WWC1	eqtl-a-ENSG00000113645	6.430851308	0.534
NPL	eqtl-a-ENSG00000135838	3.347738586	0.898
GPAT3	eqtl-a-ENSG00000138678	6.324042837	0.427
LAPTM5	eqtl-a-ENSG00000162511	0.136443524	1

Table 4. MR-PRESSO test for horizontal Pleiotropy between eQTL for 4 genes and CO.

SYMBOL	id.exposure	correct_causal_direction	steiger_pval
WWC1	eqtl-a-ENSG00000113645	TRUE	5.52E-47
NPL	eqtl-a-ENSG00000135838	TRUE	6.66E-37
GPAT3	eqtl-a-ENSG00000138678	TRUE	2.42E-05
LAPTM5	eqtl-a-ENSG00000162511	TRUE	1.11E-97

Table 5. Steiger test direction detection between eQTL for 4 genes and CO.

CO and healthy control samples (Fig. 6b). Specifically, the infiltration levels of 11 types of immune cells were significantly higher in CO samples, including CD56dim natural killer cells, gamma delta T cells, monocytes, natural killer cells, natural killer T cells, regulatory T cells, myeloid-derived suppressor cells (MDSC), etc. However, mast cell infiltration was higher in the healthy control samples. Finally, we found that the *NPL* and *WWC1* were positively correlated with these 12 differential immune cells, while *GPAT3* showed a negative correlation with these 12 differential immune cells (Fig. 6c).

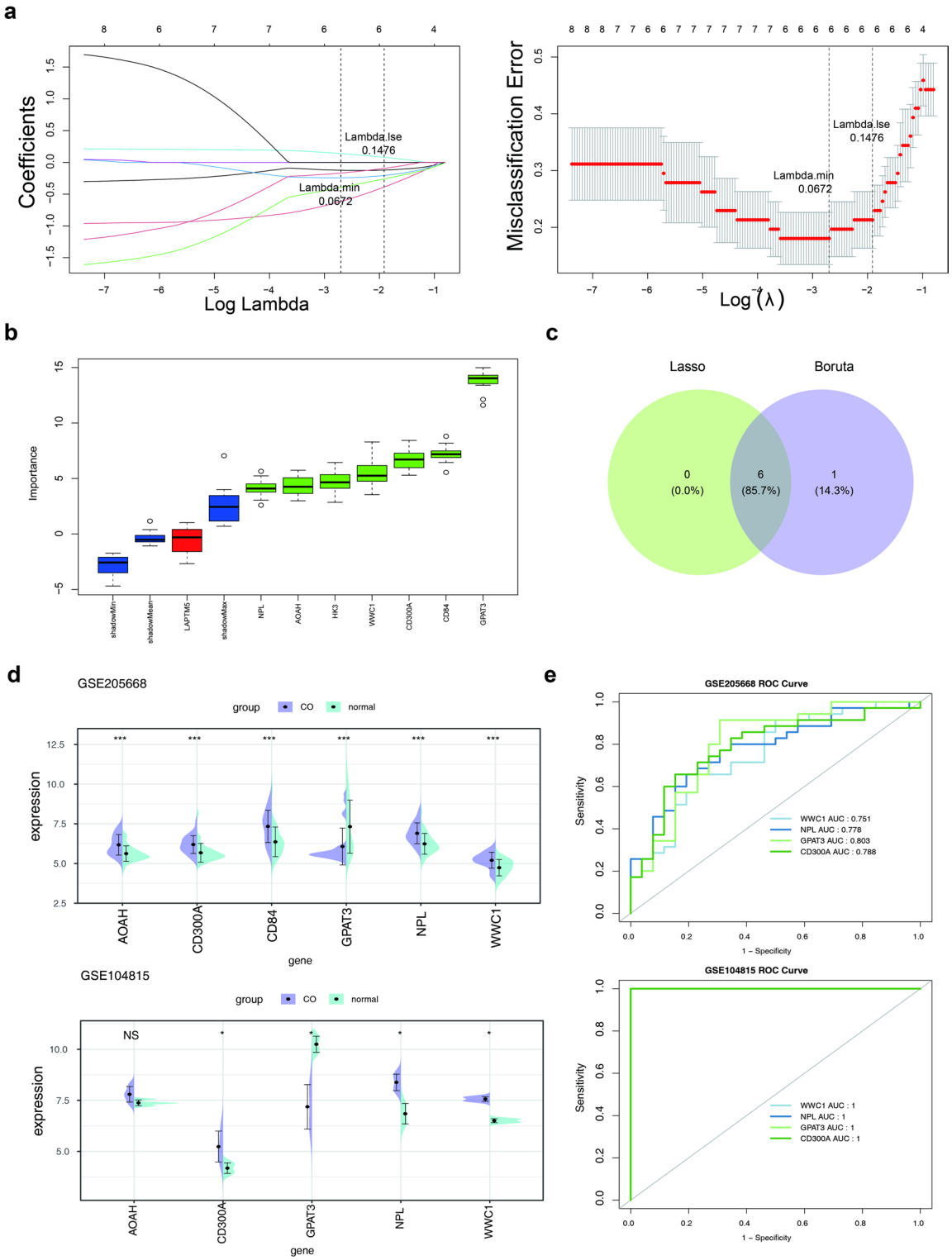

Fig. 4. Screening key genes through machine learning and verification set verification. (**a**) LASSO regression analysis, plot of gene coefficient variation with penalty coefficient, and error plot of cross validation. Each curve in the left figure represented the change trajectory of each independent variable coefficient. The vertical axis was the coefficient value, and the upper horizontal axis was the number of non - zero coefficients in the model at this time. (**b**) Boruta analysis, obtaining 3 genes with confirmed attributes (green) and their importance ranking (green is an important variable, blue is a shadow variable, and yellow is a Tentative variable). (**c**) Venn diagram of cross genes (intersection of feature genes 1 and 2 obtained by Lssso and Boruta). (**d**) Violin plot of the expression levels of cross genes in the training set and validation set (* represents $P<0.05$, ** represents $P<0.01$, *** represents $P<0.001$, **** represents $P<0.0001$). (**e**) ROC curve of key genes (AUC of ROC is between 0.1 and 1. The larger the AUC value, the higher the prediction accuracy).

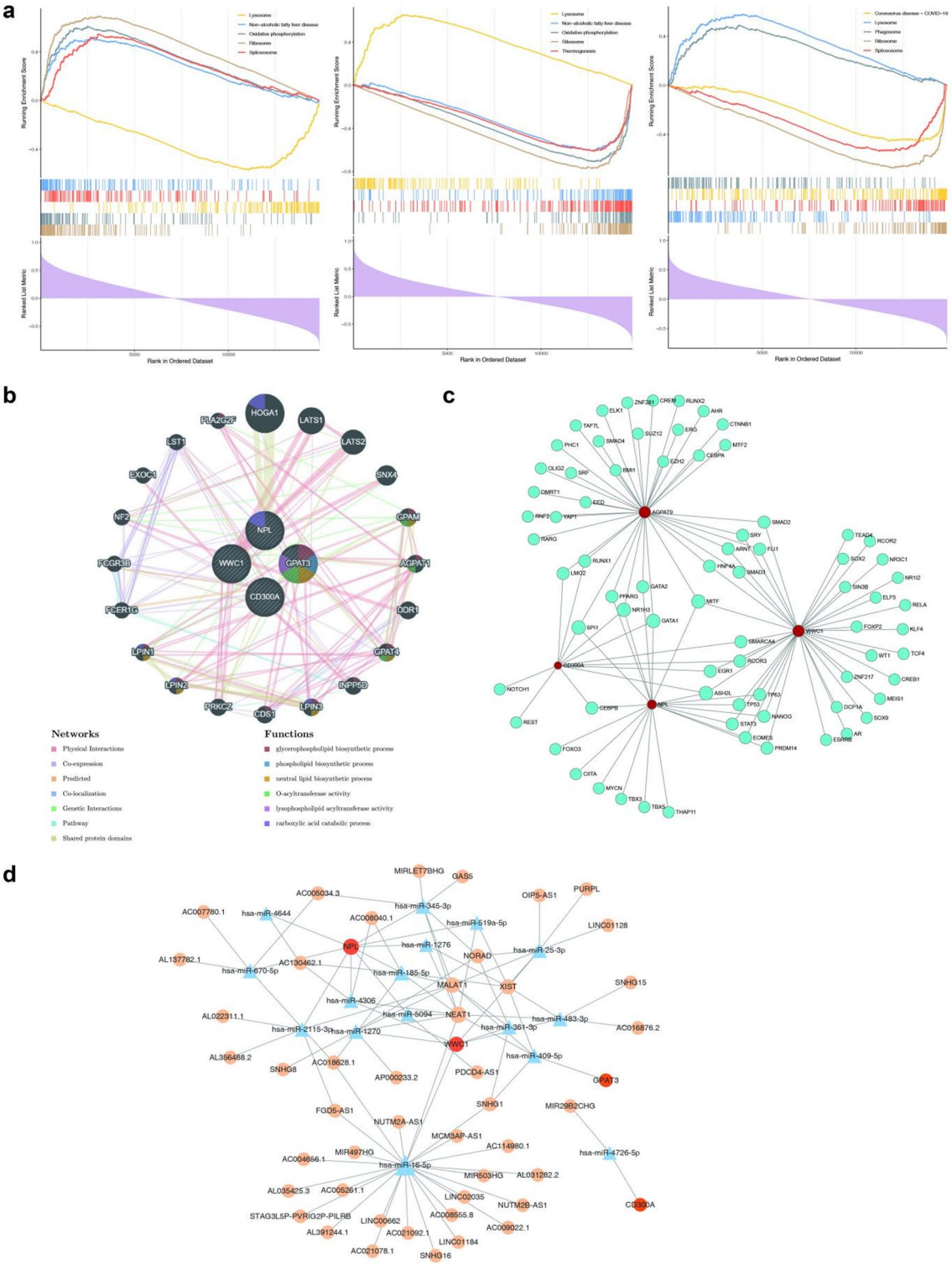

Fig. 5. GSEA analysis and regulatory network construction. (**a**) GSEA analysis of key genes (from left to right: *GPAT3*, *NPL*, *WWC1*). The horizontal axis is the background gene set sorted according to gene correlation, and the vertical axis is the corresponding Runing ES. The peak of the line graph is the enrichment score of the enrichment pathway. (**b**) Key genes, GCI network of the top 20 genes with the strongest functional similarity. (**c**) mRNA-TF network, in which yellow represents key genes and purple represents transcription factors. (**d**) ceRNA molecular regulatory network, in which yellow nodes represent key genes; pink nodes represent miRNA; cyan nodes represent lncRNA.

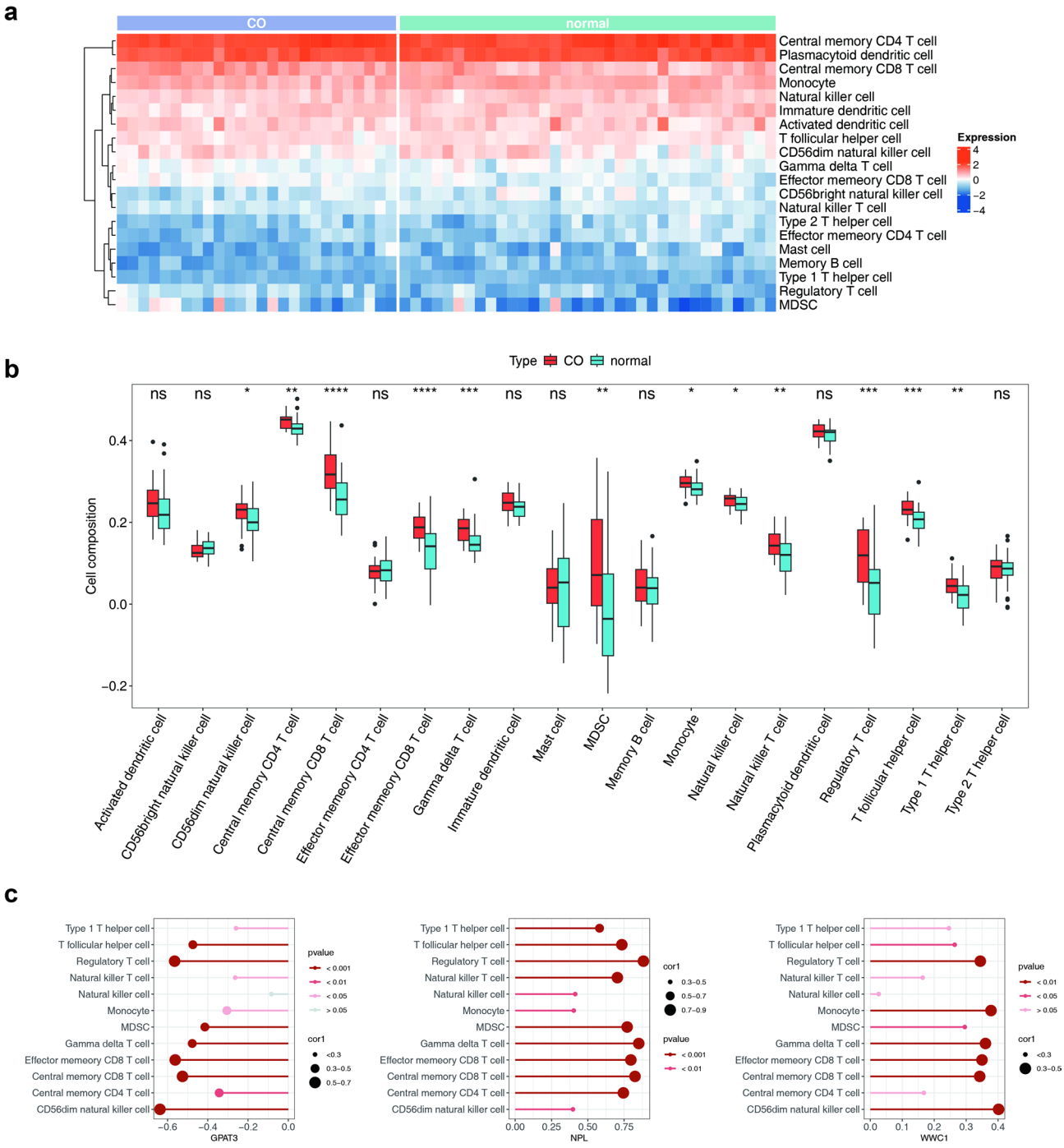

Fig. 6. Immune infiltration analysis. (**a**) Expression heat map of different immune cells in normal and disease samples. (**b**) Box plot of the difference in the proportion of immune cells, (* represents $P<0.05$, ** represents $P<0.01$, *** represents $P<0.001$, **** represents $P<0.0001$). (**c**) Lollipop plot of the correlation between key genes and differential immune cells (from left to right: *WWC1*, *NPL*, *CD300A*).

Discussion

At present, CO has become an increasingly serious public health problem worldwide. In the past three decades, the global incidence rate of obesity has doubled, affecting more than 340 million children[15]. Polyamines are multifunctional cations that are essential in almost all living organisms. Research has found a close correlation between elevated levels of polyamines in the blood and CO[12]. And this study found that *WWC1*, *NPL*, and *GPAT3* are three key genes related to CO and polyamine metabolism, and conducted preliminary research on these three key genes, and found that they may play important roles in regulating the pathophysiological processes of CO. This is the first discovery of the expression regulation of these three genes in CO, and may affect the development of obesity through different pathways. The WWC protein family includes *WWC1* (the

WW and C2 domains contain 1), *WWC2*, and *WWC3*. Among them, *WWC1* is one of the upstream regulatory proteins of the Hippo signaling pathway, also known as kidney and brain (*KIBRA*)[16].Currently, no direct association has been found between *WWC1* and obesity, but research has found that SelenoM mainly improves metabolic inflammation in obesity through the Hippo YAP/TAZ-ROS signaling axis[17].The fat, four-joint, and hippo pathway also regulate obesity and that they act in neurons, rather than in adipose tissue (fat body)[18] N-acetylneuraminpyruvate lyase (*NPL*) catalyzes the main sialic acid: N-acetylneuraminic acid- 9 - phosphate (the substrate) to N - acetylmannosamine – 6 - phosphate and pyruvate[19]. Research has shown that MRSA N - acetylneuraminpyruvate lyase (*NPL*) has a relatively high KM, indicating that the enzyme may regulate the flux through catabolic pathways[20]. A study suggests that *NPL* is crucial for muscle function and regeneration, and is a general marker of muscle injury[21] *GPAT3* is an important enzyme, whose full name is Glycerol-3-phosphate acyltransferase 3. This enzyme plays a crucial role in cells, primarily catalyzing the conversion of glycerol-3-phosphate into lysophosphatidic acid, which are precursors for the synthesis of triglyceride[22].Triglycerides are the main form of fat, which store energy in cells and provide a source of energy when needed by the body. *GPAT3* is involved in regulating the synthesis of fatty acids and lipid metabolism, which are crucial for maintaining cellular structure and function[23] .In addition, *GPAT3* is closely related to energy metabolism as it directly affects the synthesis rate of triglycerides, which in turn affects overall energy balance and weight regulation[24]. In the study, the abnormal expression of *GPAT3* is closely related to some metabolic diseases, especially obesity related diseases, such as type 2 diabetes and cardiovascular diseases[25]. Some studies have also found that GPAT3 may play a role in the development of CO by regulating the interaction between fatty acid metabolism and polyamine metabolism[26]. This study found significant differences in *WWC1*, *NPL*, and *GPAT3* between CO and the control, and a significant causal relationship with CO. Indicating that *WWC1*, *NPL*, and *GPAT3* may be potential regulatory targets for CO.

The GSEA analysis in this study showed that three key genes were co-enriched in the ribosome and lysosome pathways. Ribosomes are complex structures responsible for protein synthesis in cells, composed of ribosomal RNA (rRNA) and ribosomal protein (r-protein). The main function of the ribosome pathway is to translate mRNA into protein, which is crucial for cell growth, proliferation, and repair[27]. Research has shown that ribosomes play a role in cell proliferation, differentiation, apoptosis, and transformation, affecting the rate of protein synthesis. Ribosome abnormalities can seriously affect cell fate, leading to various ribosome related diseases such as COVID-19 virus infection, cardiovascular disease, blood disease, etc[28]. However, in obesity, abnormal cellular metabolism may lead to abnormal accumulation of adipose tissue. Dysfunction of the ribosome pathway may affect protein synthesis in cells, thereby affecting cellular metabolic function. Mutations or dysregulated expression of ribosomal proteins may affect the function and insulin sensitivity of adipocytes[28]. On the other hand, ribosomal pathway is associated with cellular stress response and may be involved in regulating inflammatory responses, which are closely related to the development of obesity[29]. Lysosomes play a crucial role in cellular homeostasis, development, and aging, serving as the cell's degradation center and signaling hub.The changes in lysosomal function are crucial for supporting cell adaptation to various signals and stimuli[30]. The acidic environment within the lysosomal lumen is sustained by the multi-subunit V-ATPase. This low pH, ranging from 4.5 to 5.5, activates over 50 intralysosomal hydrolases that break down macromolecules such as proteins, nucleic acids, lipids, and carbohydrates[30]. The functions involved in lysosomal pathways include autophagy, degradation of substances, and disposal of intracellular waste[31]. Dysfunction of autophagic lysosome reformation (*ALR*) is emerging as an important disease mechanism. This includes neurodegenerative disorders such as hereditary spastic paraplegia and Parkinson disease, neuropathies including Charcot-Marie-Tooth disease, lysosome storage disorders, muscular dystrophy, metabolic syndrome, as well as inflammatory and liver disorders[32]. Metabolic syndrome consists of hypertension, high triglycerides and low high-density lipoprotein cholesterol, excessive abdominal obesity, and high blood sugar. Among these, inhibition of ALR may also result in hepatic steatosis[33]. This is a liver component disorder known as metabolic syndrome, characterized by abnormal accumulation of fat in liver tissue. Autophagy can clear fat storage organelles called lipid droplets in liver cells ("lipophagy")[34]. It is speculated that autophagy defects related to lysosomes can lead to excessive accumulation of adipose tissue, thereby promoting the development of obesity.

Recent studies have demonstrated a connection between obesity and systemic chronic low-grade inflammation[35]. In addition, it was proposed that the disorder of inflammation is closely related to the nutritional metabolic pathway and obesity related complications (such as insulin resistance and type 2 diabetes[36].The inflammatory impacts of obesity may be systemic and can lead to metabolic disorders and cellular alterations. The low-grade inflammation associated with obesity seems to mainly originate from macrophage infiltration in adipose tissue[37]. Monocytes are an important class of immune cells that primarily play a role in inflammatory response and antimicrobial immunity[38]. They can differentiate into macrophages and participate in clearing pathogens and regulating immune responses.Under obesity conditions, the activity and quantity of monocytes may change, affecting the inflammatory state and metabolic environment of adipose tissue[39]. Studies have demonstrated that CO involves alterations in monocyte gene expression associated with obesity and increased complexity of coronary atherosclerosis in adults[40]. In addition, studies have found that chronic low-grade inflammation in CO is associated with decreased expression of IL-10 in monocyte subsets[41]. Therefore, the interaction between monocytes/macrophages and inflammatory mediators may play a crucial role in the pathogenesis of obesity.The correlation analysis of this study found that monocytes were significantly positively correlated with *NPL* and *WWC1*, and significantly negatively correlated with *GPAT3*. NPL may affect the activity of monocytes through signaling pathways or the expression of regulatory factors. *WWC1* may affect the biological function of monocytes by regulating cell apoptosis or proliferation, thereby playing a certain promoting role in the activation or function of monocytes. The expression of *GPAT3* in monocytes may be related to the negative regulation of immune response. These analyses can provide a deeper perspective on the mechanism of immune cells in CO, and provide theoretical basis for future treatment strategies and drug development.

As key genes related to childhood obesity and polyamine metabolism, *WWC1*, *NPL*, and *GPAT3* may be associated with gene expression regulation. TF is a protein that can bind to specific DNA sequences and regulate gene expression. Many TFs act as main regulatory factors and selection genes, controlling the determination of cell types, developmental patterns, and specific pathways such as immune responses. We utilized Network Analyst to identify 72 TFs corresponding to 3 key genes with MITF concurrently regulating three key genes. MITF (Microphthalmia associated transcription factor) is an important transcription factor that is typically associated with the regulation of multiple genes, particularly playing a crucial role in regulating cell differentiation, pigmentation, and immune response[42,43]. MITF has also been found to be associated with adipocyte differentiation and lipid metabolism. Research has shown that inducing the expression of glycoprotein non metastatic melanoma protein B (Gpnmb) in adipose tissue macrophages (ATM) can cause the translocation of MITF to the nucleus, and MITF plays a key role in some ATM phenotypes[44]. In summary, it is speculated that MITF can affect the function and metabolic status of adipocytes by regulating the expression of key genes (*WWC1*, *NPL*, *GPAT3*), thereby affecting the occurrence and development of CO, providing a new approach for the treatment of CO. Future research can delve into the specific regulatory mechanisms of these TFs in obesity related metabolic disorders, particularly how they affect the activity of polyamine metabolic pathways and the development of related diseases.

This study first identified key genes (*WWC1*, *NPL*, *GPAT3*) related to polyamine metabolism in CO based on bioinformatics methods at the transcriptome level, revealing the potential regulatory mechanisms of CO development, and further analyzing the molecular mechanisms by which key genes affect CO. And through MR analysis, it was found that these three key genes have a causal relationship with CO, providing new directions for the treatment of CO. But clinical applications require more sample data support. We will continue to monitor the role of these genes.

Methods

Data sources

The GSE205668 dataset (GPL16791 platform), including RNA-seq data of subcutaneous fat from 26 obese children and 35 control samples, was downloaded from the GEO database (https://www.ncbi.nlm.nih.gov/geo/) as the training cohort. The GSE104815 dataset (GPL21827 platform), consisting of transcriptome data of subcutaneous fat from 4 CO and 4 control samples, was downloaded from the GEO database as the validation cohort for external validation. Additionally, 59 PMRGs were downloaded from the Molecular Signatures Database (MSigDB, http://software.broadinstitute.org/gsea/msigdb/index.jsp). In order to present the study visually, a flowchart was drawn as shown in Fig. 7.

Screening of differentially expressed genes (DEGs) associated with CO

Differential expression analysis aims to identify the genes that are differentially expressed between different sample groups and do subsequent more in-depth functional mining of the differentially expressed genes.To identify the DEGs1 between CO and control groups, we performed differential expression analysis by the "DESeq2" (version 1.42.0)[45]. package on the training cohort (|log2Fold Change (FC)|>0.5 and false discovery rate (FDR) < 0.05). Subsequently, we used "ggplot2" (version 3.4.4)[46](ggplot2: Elegant Graphics for Data Analysis) to generate a volcano plot to visually display the results, with the top 10 DEGs based on |log2FC| highlighted. We also used the "circlize" (version 0.4.15)[47]. package to create a circular heatmap of the top 20 up-regulated and down-regulated DEGs.

Screening of DEGs related to polyamine metabolism

Consensus clustering using 59 polyamine metabolism-related genes (PMRGs) was performed to group the GO samples, which allowed the detection of gene expression changes between subtypes and led to the identification of more CO differentially expressed genes associated with polyamine metabolism. The expression data derived from 26 CO samples within the training corpus were meticulously analyzed through a consensus clustering procedure facilitated by the ConsensusClusterPlus package (version 1.66.0)[48]. The parameters selected were "maximum" and "pam" (Partitioning around, medoids). Subsequently, based on the classification results of the subtypes, differential expression analysis was executed on the different subtypes using the "DESeq2" package[45] (|log2FC|>0.5 and p.adj < 0.05) to identify subtype-specific DEGs2, where the p-value was corrected by the Benjamini - hochberg method.

Identification of candidate genes

To obtain genes related to PMRGs in CO, the intersection of two sets of DEGs was obtained using the "ggvenn" (version 0.1.10)(https://CRAN.R-project.org/package=ggvenn)(ggvenn: Draw Venn Diagram by 'ggplot2') package. The resulting intersecting genes were considered as candidate genes associated with polyamine metabolism in CO. Different subtypes may represent distinct cellular response states to polyamine metabolism in childhood obesity. Since DEGs2 are genes that show differential expression between these two subtypes, they are closely related to the changes in cellular states of polyamine metabolism in childhood obesity. The intersection of DEGs1 and DEGs2 provided us with a more targeted set of candidate genes, which were likely key factors in polyamine metabolism in childhood obesity and play an important role in disease progression.

Functional analysis

In this study, with the aim of further exploring the functions played by the candidate genes, we employed the "clusterProfiler" package (version 4.7.1.003)[49]. and the human gene annotation package "org.Hs.eg.db" (version 3.16.0)[50] executed Gene Ontology (GO) and Kyoto Encyclopedia of Genes and Genomes (KEGG) enrichment analyses on the candidate genes[51]. The significance threshold of $p < 0.05$ was adjusted using the Benjamini-

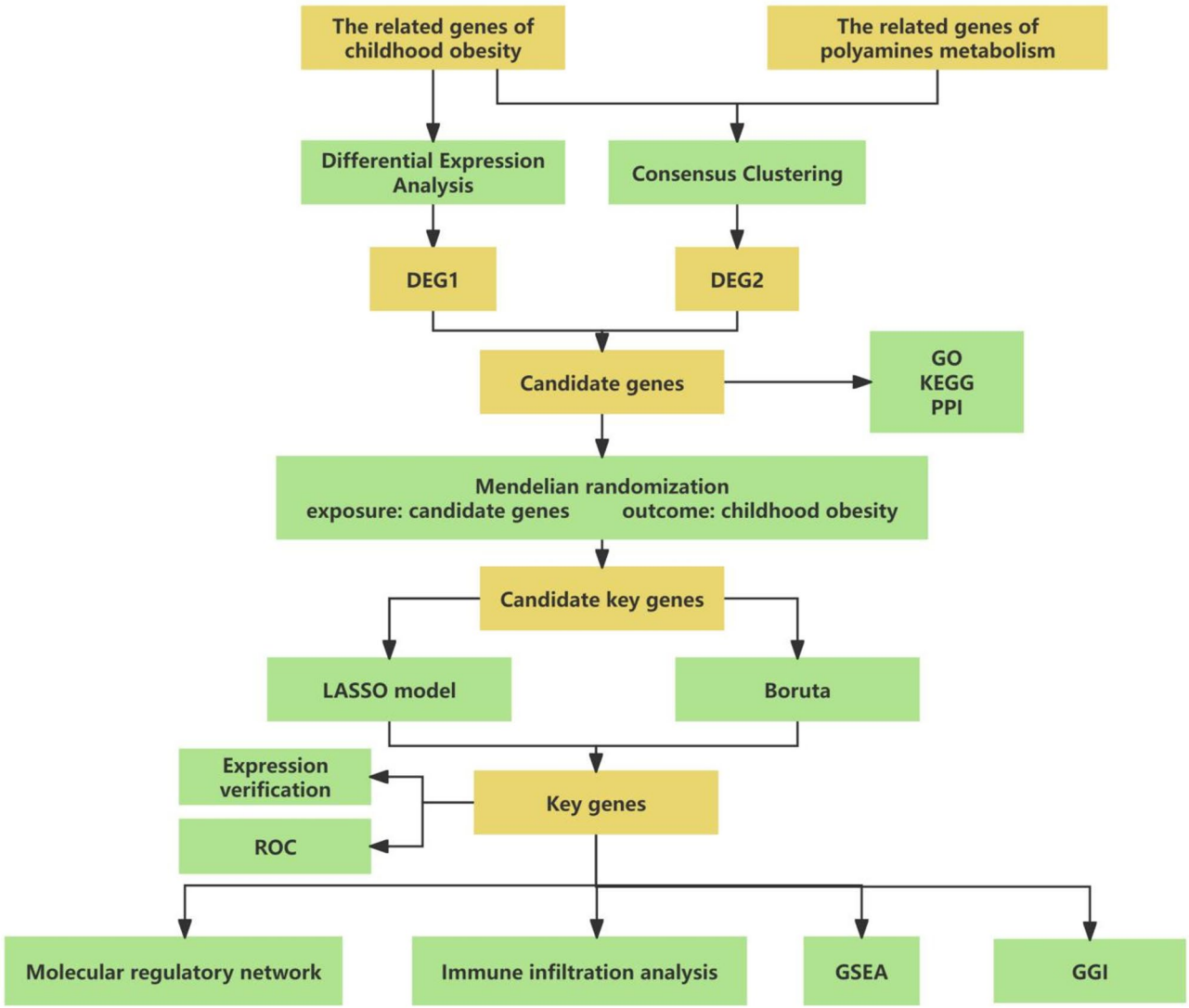

Fig. 7. Flow chart of the research programme.

Hochberg method. To explored the protein-protein interaction relationships among the candidate genes, this study utilized the String database (https://string-db.org) to build a protein-protein interaction (PPI) network of the candidate genes (confidence = 0.4), and the visualization was performed using Cytoscape (version 3.7.1)[52].

Data pre-processing for MR study

To explored the causal relationship between polyamine metabolism-related genes and CO, The MR analysis was conducted with the candidate genes as the exposure factor and CO as the outcome event to explore the causal relationship between candidate genes and CO. The 3 main assumptions of classical MR analysis were satisfied throughout the analysis: (i) the independence assumption (instrument variables [IVs] are not associated with any confounders); (ii) the association assumption (IVs directly affect exposure); (iii) the exclusivity assumption (IVs can only affect the outcome variable through exposure factors, and not through other pathways).

Firstly, the expression quantitative trait loci (eQTL) of the candidate genes was obtained from the Integrative Epidemiology Unit (IEU) Open Genome-wide association study (GWAS) database (https://gwas.mrcieu.ac.uk/) as the exposure data. Then, the outcome (CO) data also were searched in the IEU OpenGWAS database, yielding the dataset "ieu-a-1096" with the following information: sample size: 13,848 Europeans (5,530 cases and 8,318 control) and number of SNPs: 2,442,739.

First, the exposure factors were extracted and IVs that met the analysis criteria ($p < 5*10-6$) were selected using the 'extract_instruments' function in the TwoSampleMR (version 0.5.8)[53]package. The IVs with linkage disequilibrium (LD) were removed using the criteria 'clump = TRUE', 'r2 = 0.001', and 'kb = 5000'. The outcome variables were then read using the 'format_data' function in the TwoSampleMR package and filtered in combination with the IVs from the exposure factors ($p < 5*10-6$). To account for weak instrument bias, the strength of each IV was evaluated by calculating the F statistic. The formula is as follows: $F = R2\times(N-2)/(1-R2)$. In this formula, R2 is the cumulative explanatory variance of the selected IVs for the exposure factor and N is the

sample size of the GWAS data. An F statistic greater than 10 indicates no weak instrument bias and suggests the potential of the IV to predict the outcome. Finally, the 'harmonise_data' function in the TwoSampleMR package was used to standardize effect alleles and effect sizes, obtaining remained IVs for MR analysis.

MR study

MR analysis was performed using five methods: Inverse variance weighted (IVW)[54], MR Egger[55],Weighted median[56],Simple mode[53],Weighted mode[57]. In 5 methods, IVW was considered the most important methods[58]. This was mainly because it gave the highest weight to the estimates with the smallest variance, making the overall results more reliable and less affected by outliers. In contrast to other methods, IVW was better able to synthesize the information from multiple genetic variants, providing a more accurate assessment of the causal relationship under investigation[59] Therefore, in the context of exploring the causal relationship between polyamine metabolism-related genes and CO, IVW stood out as the principal approach among the five. In addition, candidate key genes were selected based on odd ratio (OR) > 1 and $\log_2$FC (log - base 2 fold - change) > 0 or OR < 1 and $\log_2$FC < 0. The rationale behind choosing genes with OR > 1 and $\log_2$FC > 0 was that an odds ratio greater than 1 indicated a positive association between the gene and the condition being studied. A $\log_2$FC greater than 0 implied that the gene's expression was up - regulated. On the other hand, for genes with OR < 1 and $\log_2$FC < 0, an odds ratio less than 1 suggested a negative association, and a negative $\log_2$FC indicated down - regulated expression[60]. Such genes may have had an inhibitory effect. Then, the correlation between the exposure factor and the outcome was determined by examining the intercept in the scatter plot. A positive slope of the fitted line indicated that the exposure was a risk factor, while a negative slope suggested that the exposure was a protective factor. Next, the 'mr_forest_plot' function was used to generate a forest plot to assess the diagnostic performance of each single nucleotide polymorphism (SNP) in estimating the exposure factor on the outcome factor. Randomness was assessed by examining the symmetry of the samples distributed on both sides of the IVW line in the funnel plot. If the samples were symmetrically distributed, the MR analysis conformed to Mendel's second law of random grouping.

To evaluate the reliability of the results, we conducted various tests. Firstly, a heterogeneity test was performed. If Q_p value > 0.05, it indicated no heterogeneity. Secondly, we used the 'MR-PRESSO' and 'MR-Egger' functions from TwoSampleMR package to assess horizontal pleiotropy. A p-value greater than 0.05 suggested the absence of horizontal pleiotropy. Thirdly, a leave-one-out (LOO) analysis was conducted. The principle of the leave-one-out analysis was to exclude one SNP and perform MR using the remaining SNPs to examine whether the excluded SNP had a significant impact on the results. Additionally, the Steiger test was used to examine whether the direction of the MR analysis was correct (correct causal direction = TRUE and steiger test $p < 0.05$). Overall, after above analyses, candidate key genes were identified.

Selection of key genes

In the training cohort, we aimed to screen the candidate key genes obtained previously through certain methods to further identify the key genes. To achieve this, we employed the glmnet (verion 4.1-8)[61] package with the family parameter set to "binomial" and the type.measure parameter set to "class" to reduce the dimensionality of features and construct a least absolute shrinkage and selection operator (LASSO)[62] model for identifying feature genes. We utilized 10-fold cross-validation to calculate error rates across a range of lambda values (from λ_min to λ_max) to identify the optimal lambda that minimized the cross-validated error. Simultaneously, in the training cohort, we performed Boruta analysis on the candidate key genes using the Boruta (version 8.0.0)[63] (Feature Selection with the Boruta Package) package, which identified the confirmed attributes (green) and ranked their importance. Finally, we took the intersection of the feature genes obtained from LASSO and Boruta, resulting in the set of intersected genes. These intersected genes hold significant importance as they represent the core genetic elements that have been consistently identified by both the LASSO[62] and Boruta methods[64]. A Venn diagram was created for visualization.

In both the training and validation cohorts, violin plots were generated to display the expression patterns of the intersected genes in samples from diseased and control groups. This was done to determine the key genes associated with polyamine metabolism in CO. Next, we conducted receiver operating characteristic (ROC) analysis using the pROC (version 1.18.5)[65] package in the validation cohort and training cohort to explore the diagnostic value of the key genes in CO.

Function analysis of key genes

We executed GSEA to identify regulatory pathways that were associated with the expression of key genes. Firstly, using the key genes as the target genes, we calculated the correlation coefficients between the key genes and all other genes in the dataset GSE205668, using "c2.cp.kegg.v7.5.1.entrez.gmt" as the background genes. We then sorted the correlations in descending order. Next, we conducted GSEA using the clusterProfiler package (version 4.10.0)[49]with the criteria |normalized enrichment score (NES)| > 1 and $p < 0.05$. Besides, we utilized the GeneMANIA database (http://www.genemania.org)[66] to obtain genes that interacted with key genes, and constructed a gene-gene interaction (GGI) network to elucidate the relationships between key genes and their interacting genes.

Molecular regulatory network

We employed NetworkAnalyst (https://www.networkanalyst.ca/) to predict the TFs that regulated the key genes, and constructed an mRNA-TF network to illustrate the interaction between key genes and TFs. Subsequently, we further explored the potential regulatory mechanisms of the key genes. Firstly, we utilized the miRWalk (http://mirwalk.umm.uni-heidelberg.de/) database to predict the target miRNAs that interacted with the key genes, and filtered out the miRNAs supported by miRDB (https://mirdb.org/). Then, we obtained the key lncRNAs upstream

of the aforementioned target miRNAs from the starbase (https://rnasysu.com/encori/) database, filtering them based on the conditions clipExpNum > 4 and pancancerNum > 6. Finally, the constructed lncRNA-miRNA-key genes molecular regulatory network was visualized using Cytoscape (version 3.8.2)[52].

Immune infiltration analysis

To comprehensively understand the immune microenvironment and its relationship with key genes in the context of the studied disease, in all samples of the dataset GSE205668, we evaluated the infiltration of 28 types of immune cells using the single-sample GSEA (ssGSEA) algorithm of the GSVA (version 1.50.0)[67] package, and visualized the results using the pheatmap package to generate a heatmap. Next, to investigate the differences in immune cell infiltration between the disease and healthy control groups ($p < 0.05$), we performed the Wilcoxon rank-sum test[68]. Box plots were generated using the ggplot2 package to illustrate the differences. Finally, we conducted Spearman correlation analysis[69] to explore the correlation between key genes and immune cells that showed significant differences ($p < 0.05$).

Statistical analysis

All analyses were conducted using the R programming language (v 4.2.3). Diversity inter-groups were seriously analyzed by Wilcoxon rank-sum test. Calibration of p-values used the Benjamini - hochberg method[70]. Additionally, the correlation analysis were calculated using Spearman analysis. P-value < 0.05 was deemed statistically meaningful unless otherwise stated.

Data availability

The datasets generated during and/or analysed during the current study are available in the [GEO database] repository, [https://www.ncbi.nlm.nih.gov/geo/, GSE104815, GSE205668]. and the Molecular Signatures Datab ase, [http://software.broadinstitute.org/gsea/msigdb/index.jsp].

Received: 8 October 2024; Accepted: 15 May 2025
Published online: 22 May 2025

References

1. Li, Q., Gao, J., Luo, J., Lin, D. & Wu, X. Mendelian randomization analyses support causal relationship between gut microbiota and childhood obesity. *Front. Pediatr.* **11**, 1229236. https://doi.org/10.3389/fped.2023.1229236 (2023).
2. Fu, Q. *The Global Epidemic of Childhood Obesity and Its Non-medical Costs*. (2015).
3. Llewellyn, A., Simmonds, M., Owen, C. G. & Woolacott, N. Childhood obesity as a predictor of morbidity in adulthood: a systematic review and meta-analysis. *Obes. Rev.* **17**, 56–67. https://doi.org/10.1111/obr.12316 (2016).
4. Milaneschi, Y. et al. Genetic association of major depression with atypical features and Obesity-Related immunometabolic dysregulations. *JAMA Psychiatry*. **74**, 1214–1225. https://doi.org/10.1001/jamapsychiatry.2017.3016 (2017).
5. Fang, X. et al. Causal association of childhood obesity with cancer risk in adulthood: A Mendelian randomization study. *Int. J. Cancer*. **149**, 1421–1425. https://doi.org/10.1002/ijc.33691 (2021).
6. Unick, J. L. et al. Evaluation of early weight loss thresholds for identifying nonresponders to an intensive lifestyle intervention. *Obes. (Silver Spring)*. **22**, 1608–1616. https://doi.org/10.1002/oby.20777 (2014).
7. Liu, J., Zhang, Y., Wang, Q. Q., Zhou, Y. & Liu, J. L. Fat body-specific reduction of CTPS alleviates HFD-induced obesity. *Elife* **12** https://doi.org/10.7554/eLife.85293 (2023).
8. May, M., Schindler, C. & Engeli, S. Modern Pharmacological treatment of obese patients. *Ther. Adv. Endocrinol. Metab.* **11**, 2042018819897527. https://doi.org/10.1177/2042018819897527 (2020).
9. Du, N. et al. Fluorescent nanoprobe array based on carbon nanodots for qualitative and quantitative determination of biogenic polyamine. *Mikrochim Acta*. **187**, 522. https://doi.org/10.1007/s00604-020-04492-4 (2020).
10. Xuan, M. et al. Polyamines: their significance for maintaining health and contributing to diseases. *Cell. Commun. Signal.* **21**, 348. https://doi.org/10.1186/s12964-023-01373-0 (2023).
11. Eisenberg, T. et al. Cardioprotection and lifespan extension by the natural polyamine spermidine. *Nat. Med.* **22**, 1428–1438. https://doi.org/10.1038/nm.4222 (2016).
12. Codoñer-Franch, P., Tavárez-Alonso, S., Murria-Estal, R., Herrera-Martín, G. & Alonso-Iglesias, E. Polyamines are increased in obese children and are related to markers of oxidative/nitrosative stress and angiogenesis. *J. Clin. Endocrinol. Metab.* **96**, 2821–2825. https://doi.org/10.1210/jc.2011-0531 (2011).
13. Jell, J. et al. Genetically altered expression of Spermidine/spermine N1-acetyltransferase affects fat metabolism in mice via acetyl-CoA. *J. Biol. Chem.* **282**, 8404–8413. https://doi.org/10.1074/jbc.M610265200 (2007).
14. Lawlor, D. A., Harbord, R. M., Sterne, J. A. & Timpson, N. Davey Smith, G. Mendelian randomization: using genes as instruments for making causal inferences in epidemiology. *Stat. Med.* **27**, 1133–1163. https://doi.org/10.1002/sim.3034 (2008).
15. Jebeile, H., Kelly, A. S., O'Malley, G. & Baur, L. A. Obesity in children and adolescents: epidemiology, causes, assessment, and management. *Lancet Diabetes Endocrinol.* **10**, 351–365. https://doi.org/10.1016/s2213-8587(22)00047-x (2022).
16. Höffken, V., Hermann, A., Pavenstädt, H., Kremerskothen, J. W. W. C. & Proteins Important regulators of Hippo signaling in Cancer. *Cancers (Basel)*. 13. https://doi.org/10.3390/cancers13020306 (2021).
17. Cai, J. et al. Hippo-YAP/TAZ-ROS signaling axis regulates metaflammation induced by SelenoM deficiency in high-fat diet-derived obesity. *J. Adv. Res.* https://doi.org/10.1016/j.jare.2024.06.005 (2024).
18. Agrawal, N. et al. Predicting novel candidate human obesity genes and their site of action by systematic functional screening in Drosophila. *PLoS Biol.* **19**, e3001255. https://doi.org/10.1371/journal.pbio.3001255 (2021).
19. Xiao, S., Li, R., Diao, H., Zhao, F. & Ye, X. Progesterone receptor-mediated regulation of N-acetylneuraminate pyruvate lyase (NPL) in mouse uterine luminal epithelium and nonessential role of NPL in uterine function. *PLoS One*. **8**, e65607. https://doi.org/10.1371/journal.pone.0065607 (2013).
20. North, R. A. et al. Structure and Inhibition of N-acetylneuraminate lyase from methicillin-resistant Staphylococcus aureus. *FEBS Lett.* **590**, 4414–4428. https://doi.org/10.1002/1873-3468.12462 (2016).
21. Da Silva, A. et al. N-acetylneuraminate pyruvate lyase controls sialylation of muscle glycoproteins essential for muscle regeneration and function. *Sci. Adv.* **9**, eade6308. https://doi.org/10.1126/sciadv.ade6308 (2023).
22. Shan, D. et al. GPAT3 and GPAT4 are regulated by insulin-stimulated phosphorylation and play distinct roles in adipogenesis. *J. Lipid Res.* **51**, 1971–1981. https://doi.org/10.1194/jlr.M006304 (2010).
23. Lu, B. et al. Expression and regulation of GPAT isoforms in cultured human keratinocytes and rodent epidermis. *J. Lipid Res.* **51**, 3207–3216. https://doi.org/10.1194/jlr.M007054 (2010).

24. Cao, J., Li, J. L., Li, D., Tobin, J. F. & Gimeno, R. E. Molecular identification of microsomal acyl-CoA:glycerol-3-phosphate acyltransferase, a key enzyme in de Novo triacylglycerol synthesis. *Proc. Natl. Acad. Sci. U S A*. **103**, 19695–19700. https://doi.org/10.1073/pnas.0609140103 (2006).
25. Cao, J. et al. Mice deleted for GPAT3 have reduced GPAT activity in white adipose tissue and altered energy and cholesterol homeostasis in diet-induced obesity. *Am. J. Physiol. Endocrinol. Metab.* **306**, E1176–1187. https://doi.org/10.1152/ajpendo.00666.2013 (2014).
26. Huang, Y., Hu, K., Lin, S. & Lin, X. Glycerol-3-phosphate acyltransferases and metabolic syndrome: recent advances and future perspectives. *Expert Rev. Mol. Med.* **24**, e30. https://doi.org/10.1017/erm.2022.23 (2022).
27. Elhamamsy, A. R., Metge, B. J., Alsheikh, H. A., Shevde, L. A. & Samant, R. S. Ribosome biogenesis: A central player in Cancer metastasis and therapeutic resistance. *Cancer Res.* **82**, 2344–2353. https://doi.org/10.1158/0008-5472.Can-21-4087 (2022).
28. Jiao, L. et al. Ribosome biogenesis in disease: new players and therapeutic targets. *Signal. Transduct. Target. Ther.* **8**, 15. https://doi.org/10.1038/s41392-022-01285-4 (2023).
29. Temaj, G. et al. P53: A key player in diverse cellular processes including nuclear stress and ribosome biogenesis, highlighting potential therapeutic compounds. *Biochem. Pharmacol.* **226**, 116332. https://doi.org/10.1016/j.bcp.2024.116332 (2024).
30. Yang, C. & Wang, X. Lysosome biogenesis: regulation and functions. *J. Cell. Biol.* **220** https://doi.org/10.1083/jcb.202102001 (2021).
31. Tian, X., Teng, J. & Chen, J. New insights regarding SNARE proteins in autophagosome-lysosome fusion. *Autophagy* **17**, 2680–2688. https://doi.org/10.1080/15548627.2020.1823124 (2021).
32. Nanayakkara, R. et al. Autophagic lysosome reformation in health and disease. *Autophagy* **19**, 1378–1395. https://doi.org/10.1080/15548627.2022.2128019 (2023).
33. Schulze, R. J. et al. Lipid droplet breakdown requires dynamin 2 for vesiculation of autolysosomal tubules in hepatocytes. *J. Cell. Biol.* **203**, 315–326. https://doi.org/10.1083/jcb.201306140 (2013).
34. Lin, C. W. et al. Pharmacological promotion of autophagy alleviates steatosis and injury in alcoholic and non-alcoholic fatty liver conditions in mice. *J. Hepatol.* **58**, 993–999. https://doi.org/10.1016/j.jhep.2013.01.011 (2013).
35. Bleau, C., Karelis, A. D., St-Pierre, D. H. & Lamontagne, L. Crosstalk between intestinal microbiota, adipose tissue and skeletal muscle as an early event in systemic low-grade inflammation and the development of obesity and diabetes. *Diabetes Metab. Res. Rev.* **31**, 545–561. https://doi.org/10.1002/dmrr.2617 (2015).
36. Ip, B. et al. Th17 cytokines differentiate obesity from obesity-associated type 2 diabetes and promote TNFα production. *Obes. (Silver Spring)*. **24**, 102–112. https://doi.org/10.1002/oby.21243 (2016).
37. Weisberg, S. P. et al. Obesity is associated with macrophage accumulation in adipose tissue. *J. Clin. Invest.* **112**, 1796–1808. https://doi.org/10.1172/jci19246 (2003).
38. Coillard, A. & Segura, E. In vivo Differentiation of Human Monocytes. *Front Immunol* 10, (1907). (2019) https://doi.org/10.3389/fimmu.2019.01907
39. Kapellos, T. S. et al. Human monocyte subsets and phenotypes in major chronic inflammatory diseases. *Front. Immunol.* **10**, 2035. https://doi.org/10.3389/fimmu.2019.02035 (2019).
40. Keustermans, G. C. et al. Monocyte gene expression in childhood obesity is associated with obesity and complexity of atherosclerosis in adults. *Sci. Rep.* **7**, 16826. https://doi.org/10.1038/s41598-017-17195-3 (2017).
41. Mattos, R. T. et al. Chronic Low-Grade inflammation in childhood obesity is associated with decreased IL-10 expression by monocyte subsets. *PLoS One*. **11**, e0168610. https://doi.org/10.1371/journal.pone.0168610 (2016).
42. Gelmi, M. C., Houtzagers, L. E., Strub, T., Krossa, I. & Jager, M. J. MITF in normal melanocytes, cutaneous and uveal melanoma: A delicate balance. *Int. J. Mol. Sci.* **23** https://doi.org/10.3390/ijms23116001 (2022).
43. Louphrasitthiphol, P. et al. Acetylation reprograms MITF target selectivity and residence time. *Nat. Commun.* **14**, 6051. https://doi.org/10.1038/s41467-023-41793-7 (2023).
44. Gabriel, T. L. et al. Lysosomal stress in obese adipose tissue macrophages contributes to MITF-dependent Gpnmb induction. *Diabetes* **63**, 3310–3323. https://doi.org/10.2337/db13-1720 (2014).
45. Love, M. I., Huber, W. & Anders, S. Moderated Estimation of fold change and dispersion for RNA-seq data with DESeq2. *Genome Biol.* **15**, 550. https://doi.org/10.1186/s13059-014-0550-8 (2014).
46. Villanueva, R. A. M. & Chen, Z. J. ggplot2: elegant graphics for data analysis. *Measurement: Interdisciplinary Res. Perspect.* **17**, 160–167. https://doi.org/10.1080/15366367.2019.1565254 (2019). 2nd ed.
47. Gu, Z., Gu, L., Eils, R., Schlesner, M. & Brors, B. Circlize implements and enhances circular visualization in R. *Bioinformatics* **30**, 2811–2812. https://doi.org/10.1093/bioinformatics/btu393 (2014).
48. Wilkerson, M. D. & Hayes, D. N. ConsensusClusterPlus: a class discovery tool with confidence assessments and item tracking. *Bioinformatics* **26**, 1572–1573. https://doi.org/10.1093/bioinformatics/btq170 (2010).
49. Wu, T. et al. ClusterProfiler 4.0: A universal enrichment tool for interpreting omics data. *Innov. (Camb).* **2**, 100141. https://doi.org/10.1016/j.xinn.2021.100141 (2021).
50. Marc Carlson. org.Hs.eg.db: Genome wide annotation for Human. Rpackage version 3.12.0. (2020).
51. Kanehisa, M., Furumichi, M., Sato, Y., Kawashima, M. & Ishiguro-Watanabe, M. KEGG for taxonomy-based analysis of pathways and genomes. *Nucleic Acids Res.* **51**, D587–d592. https://doi.org/10.1093/nar/gkac963 (2023).
52. Shannon, P. et al. Cytoscape: a software environment for integrated models of biomolecular interaction networks. *Genome Res.* **13**, 2498–2504. https://doi.org/10.1101/gr.1239303 (2003).
53. Hemani, G. et al. The MR-Base platform supports systematic causal inference across the human phenome. *Elife* **7** https://doi.org/10.7554/eLife.34408 (2018).
54. Bowden, J., Davey Smith, G. & Burgess, S. Mendelian randomization with invalid instruments: effect Estimation and bias detection through Egger regression. *Int. J. Epidemiol.* **44**, 512–525. https://doi.org/10.1093/ije/dyv080 (2015).
55. Bowden, J., Davey Smith, G., Haycock, P. C. & Burgess, S. Consistent Estimation in Mendelian randomization with some invalid instruments using a weighted median estimator. *Genet. Epidemiol.* **40**, 304–314. https://doi.org/10.1002/gepi.21965 (2016).
56. Burgess, S., Butterworth, A. & Thompson, S. G. Mendelian randomization analysis with multiple genetic variants using summarized data. *Genet. Epidemiol.* **37**, 658–665. https://doi.org/10.1002/gepi.21758 (2013).
57. Hartwig, F. P., Davey Smith, G. & Bowden, J. Robust inference in summary data Mendelian randomization via the zero modal Pleiotropy assumption. *Int. J. Epidemiol.* **46**, 1985–1998. https://doi.org/10.1093/ije/dyx102 (2017).
58. Xu, J. et al. Genetic causal association between Iron status and osteoarthritis: A Two-Sample Mendelian randomization. *Nutrients* **14** https://doi.org/10.3390/nu14183683 (2022).
59. Bowden, J. & Holmes, M. V. Meta-analysis and Mendelian randomization: A review. *Res. Synth. Methods*. **10**, 486–496. https://doi.org/10.1002/jrsm.1346 (2019).
60. Zhang, X. et al. Identification of a novel immune-related transcriptional regulatory network in sarcopenia. *BMC Geriatr.* **23**, 463. https://doi.org/10.1186/s12877-023-04152-1 (2023).
61. Engebretsen, S. & Bohlin, J. Statistical predictions with Glmnet. *Clin. Epigenetics*. **11**, 123. https://doi.org/10.1186/s13148-019-0730-1 (2019).
62. Friedman, J., Hastie, T. & Tibshirani, R. Regularization paths for generalized linear models via coordinate descent. *J. Stat. Softw.* **33**, 1–22 (2010).
63. Kursa, M. B. & Rudnicki, W. R. Feature selection with the Boruta package. *J. Stat. Softw.* **36**, 1–13. https://doi.org/10.18637/jss.v036.i11 (2010).

64. Alexakis, A. & Biferale, L. λ-Navier-Stokes turbulence. *Philos. Trans. Math. Phys. Eng. Sci.* **380**, 20210243. https://doi.org/10.1098/rsta.2021.0243 (2022).
65. Robin, X. et al. pROC: an open-source package for R and S + to analyze and compare ROC curves. *BMC Bioinform.* **12**, 77. https://doi.org/10.1186/1471-2105-12-77 (2011).
66. Franz, M. et al. GeneMANIA update 2018. *Nucleic Acids Res.* **46**, W60–w64. https://doi.org/10.1093/nar/gky311 (2018).
67. Hänzelmann, S., Castelo, R. & Guinney, J. GSVA: gene set variation analysis for microarray and RNA-seq data. *BMC Bioinform.* **14**, 7. https://doi.org/10.1186/1471-2105-14-7 (2013).
68. Wilcoxon, F. in *Breakthroughs in Statistics: Methodology and Distribution* (eds Samuel Kotz & Norman L. Johnson) 196–202Springer New York, (1992).
69. Spearman, C. The proof and measurement of association between two things. *Int. J. Epidemiol.* **39**, 1137–1150. https://doi.org/10.1093/ije/dyq191 (2010).
70. Haynes, W. in *Encyclopedia of Systems Biology* (eds Werner Dubitzky, Olaf Wolkenhauer, Kwang-Hyun Cho, & Hiroki Yokota) 78–78Springer New York, (2013).

Acknowledgements

We would like to express our sincere gratitude to all individuals and organizations who supported and assisted us throughout this research. Without your support, this research would not have been possible. Thanks to the Natural Science Foundation of Jiangsu Province (No. BK20240297） for help with this study.

Author contributions

MM S, P Z, S Y. conceived the experiment(s), MM S, YY Q, X P S. conducted the experiment(s), MM S.， JL J and L D. analysed the results. All authors reviewed the manuscript.

Declarations

Competing interests

The authors declare no competing interests.

Additional information

Correspondence and requests for materials should be addressed to J.J. or L.D.

Reprints and permissions information is available at www.nature.com/reprints.

Publisher's note Springer Nature remains neutral with regard to jurisdictional claims in published maps and institutional affiliations.